Kalman tracking and estimation of continuous gravitational waves with a pulsar timing array

Kimpson[1], Melatos, O'Leary, Evans, others, etc. etc. ⋆†
[1]Royal Astronomical Society, Burlington House, Piccadilly, London W1J 0BQ, UK

Last updated 4 July 2023

ABSTRACT

This is an abstract

Key words: gravitational waves – methods: data analysis – pulsars: general

1 INTRODUCTION

The inspiral of supermassive black hole binaries (SMBHBs; Rajagopal & Romani 1995; Jaffe & Backer 2003; Wyithe & Loeb 2003; Sesana 2013; McWilliams et al. 2014; Ravi et al. 2015; Burke-Spolaor et al. 2019; Sykes et al. 2022) is predicted to emit nHz gravitational waves (GWs). Other GW sources in this low-frequency regime include cosmic strings (e.g. Sanidas et al. 2012) and cosmological phase transitions (e.g. Xue et al. 2021). The detection of nHz GWs has necessitated the development of new observational methods, since it is practically impossible to engineer interferometric detectors with sufficiently long baselines. The foremost method is timing an ensemble of pulsars; a pulsar timing array (PTA; Tiburzi 2018; Verbiest et al. 2021). A nHz GW influences the trajectory and frequency of radio pulses, leaving a characteristic impression on the pulse times of arrival (TOAs) measured at the Earth. By measuring TOAs from multiple pulsars simultaneously one can effectively construct a detector with a baseline on the scale of parsecs. Multiple PTA detectors have been built over the last few decades, including the North American Nanohertz Observatory for Gravitational Waves (NANOGrav, Agazie et al. 2023), the Parkes Pulsar Timing array (PPTA Zic et al. 2023), and the European Pulsar Timing Array (EPTA, Antoniadis et al. 2023). These individual efforts have joined in international collaboration, under the umbrella of the International Pulsar Timing Array (IPTA, Perera et al. 2019), along with a number of newer PTAs such as the Indian Pulsar Timing Array Project (InPTA, Tarafdar et al. 2022), MeerTime (Bailes et al. 2020; Spiewak et al. 2022) and the Chinese PTA (Hobbs et al. 2019).

TK: Content and references need to be updated in light of recent PTA results. The incoherent superposition of multiple SMBHB sources leads to a stochastic GW background detectable at nHz frequencies (Allen 1997; Sesana et al. 2008; Christensen 2019; Renzini et al. 2022). Previous efforts have mainly focused on detecting the stochastic background by measuring the cross-correlation between the pulsar timing residuals between pairs of pulsars as a function of the angular separation between the pulsars – the Hellings-Downs curve (Hellings & Downs 1983). However, no GW background has yet been detected (Lentati et al. 2015; Arzoumanian et al. 2018; Antoniadis et al. 2022).

Individual SMBHBs that are sufficiently massive and nearby may be resolvable with PTAs, allowing the very earliest stages of their evolution and coalescence to be investigated (Sesana & Vecchio 2010; Yardley et al. 2010; Zhu et al. 2015; Babak & Sesana 2012; Ellis 2013; Zhu et al. 2016). Indeed, the stochastic GW background itself may be dominated by a few individual binary sources (Ravi et al. 2012). Individual SMBHBs are continuous wave sources: they generate persistent, quasi-monochromatic modulations of a known form in pulsar timing residuals. Consequently, they are detected more efficiently by either a frequentist matched filter e.g. the $\mathcal{F}$-statistic (Lee et al. 2011; Ellis et al. 2012; Zhu et al. 2014) or else Bayesian inference (Ellis & Cornish 2016; Arzoumanian et al. 2020a) rather than by cross-correlating pulsar pairs. However, PTA observational efforts to detect individual sources have thus far been unsuccessful (Jenet et al. 2004; Zhu et al. 2014; Babak et al. 2016; Arzoumanian et al. 2023).

Intrinsic pulsar timing noise – i.e. random, unmodelled, red-spectrum TOA fluctuations due to irregularities in the rotation of the star – has been identified as a key factor limiting the sensitivity of PTAs to GW signals (Shannon & Cordes 2010; Lasky et al. 2015; Caballero et al. 2016; Goncharov et al. 2021). This timing noise has multiple theorized causes including free precession (Kerr et al. 2015; Stairs et al. 2000), microglitches (D'Alessandro et al. 1995; Melatos et al. 2008; Espinoza et al. 2021), asteroid encounters (Shannon et al. 2013; Brook et al. 2013), glitch recovery (Johnston & Galloway 1999; Hobbs et al. 2010), fluctuations in internal and external stochastic torques (Cordes & Greenstein 1981; Urama et al. 2006; Antonelli et al. 2023), variations in the coupling between the stellar crust and core (Jones 1990; Meyers et al. 2021b; Melatos et al. 2021), magnetospheric state switching (Kramer et al. 2006; Lyne et al. 2010; Stairs et al. 2019) and superfluid turbulence (Greenstein 1970; Peralta et al. 2006; Melatos & Link 2014). In order to mitigate the impact of timing noise, PTAs are typically composed of millisecond pulsars (MSPs) which are relatively stable rotators. However, timing noise in MSPs may be a latent

⋆ Contact e-mail: tom.kimpson@unimelb.edu.au
† Present address: Science magazine, AAAS Science International, 82-88 Hills Road, Cambridge CB2 1LQ, UK

phenomenon that will increasingly assert itself as longer stretches of more sensitive data are analysed in the quest to detect nHz GWs (Shannon & Cordes 2010). In modern Bayesian PTA searches, the power spectral density of the intrinsic timing noise is modeled (usually as a broken or unbroken power law) and estimated, in an effort to distinguish it from the red noise induced by a stochastic GW background (whose spectrum is also red). In addition to the red timing noise there are also secondary, white noise sources that must be considered such as phase jitter noise and radiometer noise (Cordes & Shannon 2010; Lam et al. 2019; Parthasarathy et al. 2021).

In this work we present an alternative and complementary approach to PTA data analysis for individual, quasi-monochromatic, SMBHB sources which self-consistently tracks the intrinsic timing noise in PTA pulsars and disentangles it from GW-induced TOA modulations. The new approach differs from existing approaches in one key respect: it infers the GW parameters conditional on the unique, time-ordered realization of the noisy TOAs observed, instead of fitting for the ensemble-averaged statistics of the TOA noise process, e.g., the amplitude and exponent of its power spectral density. Stated another way, existing approaches seek to detect a GW signal by marginalizing over the ensemble of possible noise realizations, whereas the new approach delivers the most likely set of GW parameters consistent with the actual, observed noise realization. The new and existing approach are therefore complementary, but the new approach holds out the promise of somewhat higher sensitivity — a promise which we aim to test as the key goal of this paper. In particular, we formulate PTA analysis as a state-space problem and demonstrate how to optimally estimate the state-space evolution using a Kalman filter, a tried-and-tested tool (Kalman 1960; Meyers et al. 2021b; Melatos et al. 2021). We combine the Kalman tracking of the pulsars intrinsic rotational state with a Bayesian nested sampler (Skilling 2006; Ashton et al. 2022) to estimate the GW parameters and calculate the marginal likelihood for model selection.TK: a few extra sentences here on how we compare to existing approaches. Not quite sure yet how to do this.

This paper is organised as follows. In Section 2 we present the state-space model for the pulsar pulse frequency which is subject the influence of a GW. In Section 3 we discretise the model, develop a Kalman filter to track the state evolution and introduce how to deploy the Kalman filter in conjunction with nested sampling to estimate the system parameters and the model evidence. TK: this paper outline section will be completed once we have finalized the rest of the manuscript In Section 4 we test this new method on synthetic pulsar data. Throughout this work we adopt the natural units, with $c = G = \hbar = 1$, and a $(-,+,+,+)$ metric signature.

2 STATE-SPACE FORMULATION

We formulate the PTA analysis as a state-space problem, in which the intrinsic rotational state of each pulsar evolves according to a stochastic differential equation and is related to the observed pulse sequence via a measurement equation. In this work we take the intrinsic state variable to be the pulsar's spin frequency $f_{\rm p}^{(n)}(t)$, as measured in the local rest frame of the pulsar's centre of mass. A model for the evolution of $f_{\rm p}^{(n)}(t)$ is presented in Section 2.1. We take the measurement variable to be the radio pulse frequency measured by an observer at Earth, $f_{\rm m}^{(n)}(t)$. The measurement equation relating $f_{\rm m}^{(n)}(t)$ to $f_{\rm p}^{(n)}(t)$ is presented in Section 2.2. The superscript $1 \leqslant n \leqslant N$ indexes the n-th pulsar in the array.

2.1 Spin evolution

A predictive, first-principles theory of timing noise does not exist at present; there are several plausible physical mechanisms, referenced in Section 1. We therefore rely on an idealized phenomenological model to capture the main qualitative features of a typical PTA pulsar's observed spin evolution, i.e. random, small-amplitude excursions around a smooth, secular trend. In the model, $f_{\rm p}^{(n)}(t)$ evolves according to the sum of a deterministic torque and a stochastic torque. The deterministic torque is attributed to magnetic dipole braking, with braking index $n_{\rm em} = 3$. Most PTAs involve millisecond pulsars, for which the quadratic correction due to $n_{\rm em}$ in $f_{\rm p}^{(n)}(t)$ is negligible over the observation time $T_{\rm obs} \sim 10\,$yr, and the deterministic evolution can be approximated accurately by

$$f_{\rm em}^{(n)}(t) = f_{\rm em}^{(n)}(t_1) + \dot{f}_{\rm em}^{(n)}(t_1)t \,, \tag{1}$$

where an overdot denotes a derivative with respect to t and t_1 labels the time of the first TOA. The stochastic torque is assumed to be a zero-mean white noise process. Specifically, the frequency evolves according to an Ornstein-Uhlenbeck process, described by a Langevin equation with a time-dependent drift term (Vargas & Melatos 2023)

$$\frac{df_{\rm p}^{(n)}}{dt} = -\gamma^{(n)}[f_{\rm p}^{(n)} - f_{\rm em}^{(n)}(t)] + \dot{f}_{\rm em}^{(n)} + \xi^{(n)}(t) \,. \tag{2}$$

In Eq 2 $f_{\rm EM}$ is the solution of the electromagnetic spindown equation, $\dot{f}_{\rm EM}$ is the spin derivative, $\gamma^{(n)}$ a proportionality constant whose reciprocal specifies the mean-reversion timescale, and $\xi^{(n)}(t)$ satisfies:

$$\langle \xi^{(n)}(t) \rangle = 0 \,, \tag{3}$$

$$\langle \xi^{(n)}(t)\xi^{(n)}(t') \rangle = [\sigma^{(n)}]^2 \delta(t - t') \,. \tag{4}$$

$[\sigma^(n)]^2$ is the variance of $\xi^{(n)}$ and parametrizes the amplitude of the noise, and combined with the mean reversion it gives a characteristic root mean square fluctuations $\approx [\sigma^{(n)}]^2/\gamma^{(n)}$ in $f_{\rm p}^{(n)}(t)$ (Gardiner 2009). It is important to note that the white noise fluctuations in $\xi(t)$ translate into red noise fluctuations in the rotational phase $\phi(t) = \int_{t_1}^{t} dt'\, f_{\rm p}(t')$ after being filtered by the terms involving d/dt and γ in Eq. 1, consistent with the observed power spectral density of typical millisecond pulsars in the nHz band relevant to PTA experiments.

Equations 1–4 represent a phenomenological model, which aims to reproduce qualitatively the typical timing behaviour observed in PTAs, viz. a mean-reverting random walk about a secular spin-down trend [ref latest results paper from each of the three main PTAs]. Equations 1–4 are not derived from first principles by applying a microphysical theory. As a first pass, they also exclude certain phenomenological elements, which are likely to be present in reality, e.g. the classic, two-component, crust-superfluid structure inferred from post-glitch recoveries (Baym et al. 1969; van Eysden & Melatos 2010; Gügercinoğlu & Alpar 2017). An approach akin to Equations 1–4 has been followed successfully in other timing analyses in the context of anomalous braking indices (Vargas & Melatos 2023) and hidden Markov model glitch searches (Melatos et al. 2020; Lower

et al. 2021; Dunn et al. 2022, 2023). However, Equations 1–4 involve significant idealizations, which must be recognized at the outset (Meyers et al. 2021b,a; Vargas & Melatos 2023). First, the white noise driver $\xi(t)$ in Equation 2 is not differentiable, which makes the formal interpretation of $d^2 f_\mathrm{p}/dt^2$ ambiguous, even though $d^2 f_\mathrm{p}/dt^2$ is not used in the PTA analysis proposed in this paper. Second, the white spectrum assumed for $\xi(t)$ may or may not be suitable for millisecond pulsars in PTAs. It is challenging observationally to infer the spectrum of $\xi(t)$ from the observed spectrum of the phase residuals, because the inference is conditional on the (unknown) dynamical model governing df_p/dt. For small-amplitude fluctuations sampled relatively often, as in millisecond pulsars in PTAs, it is likely that $\xi(t)$ is white to a good approximation over the inter-TOA intervals and generates red phase residuals as observed, but caution is warranted nevertheless. Third, the Brownian increment $dB(t) = \xi(t)dt$ does not include non-Gaussian excursions such as Lévy flights (Sornette 2004) which have not been ruled out by pulsar timing experiments to date. The above three idealizations are supplemented by other, physical approximations noted above, e.g. neglecting n_em in Equation 1 and differential rotation between the crust and superfluid in Equation 2.

2.2 Modulation of pulse TOAs by a GW

In the presence of a GW, the pulse frequency measured by an observer in the local rest frame of the neutron star's center of mass is different from that measured by an observer on Earth. Indeed, the pulse TOAs are modulated harmonically at the GW frequency. We derive the nonlinear measurement equation relating $f_\mathrm{m}(t)$ to $f_\mathrm{p}(t)$ in this section. The measurement equation is a key input into the Kalman filter in Section 3.1

2.2.1 *Plane GW perturbation*

We consider a gravitational plane wave from a single,distant source, which perturbs a background Minkowski metric $\eta_{\mu\nu}$ as

$$g_{\mu\nu} = \eta_{\mu\nu} + H_{\mu\nu} \exp\left[i(\Omega(\boldsymbol{n}\cdot\boldsymbol{x} - t) + \Phi_0)\right] , \tag{5}$$

with spatial coordinates $\boldsymbol{x}$ and global coordinate time t. The GW has a constant angular frequency Ω, propagates in the $\boldsymbol{n}$-direction (where $\boldsymbol{n}$ is a unit vector), has amplitude tensor $H_{\mu\nu}$, and has a phase offset Φ_0. Throughout this paper we will work with pulsar TOAs which have been defined relative to the Solar System barycentre (SSB). We are free to choose our coordinate system such that Φ_0 is the GW phase at $t = 0$ at the SSB. In this paper Ω has no time dependence; the source is approximated as monochromatic. Studies of SMBHB inspirals in the PTA context show that the gravitational wave frequency f_gw ($= \Omega/2\pi$) evolves over decadal timescales as (e.g. Zhu et al. 2015),

$$\Delta f_\mathrm{gw} \simeq 3.94\mathrm{nHz}\left(\frac{M_c}{10^9 M_\odot}\right)^{5/3}\left(\frac{f_\mathrm{gw}(t=0)}{10^{-7}\ \mathrm{Hz}}\right)^{11/3}\left(\frac{T_\mathrm{obs}}{10\mathrm{yr}}\right) \tag{6}$$

where M_c is the chirp mass of the SMBHB, $f_{gw}(t = 0)$ is the GW frequency at the time of the first observation, and T_obs the length of the data timespan, which for PTAs is $\sim$ 10 years. A source can be considered as monochromatic if Δf_gw is less than the PTA frequency resolution of $1/T_\mathrm{obs}$. From Eq. 6 we can see that only those binaries which are very massive or at very high frequency experience significant frequency evolution over typical PTA timespans. The majority of SMBHBs detectable with PTAs are expected to satisfy $\Delta f_\mathrm{gw} < 1/T_\mathrm{obs}$; for a PTA with pulsars at 1.5 kpc, 78 % of simulated SMBHBs satisfy this condition for the current IPTA, whilst for the second phase of the Square Kilometer Array (SKA2) this fraction drops to 52 % (Fig 7 of Rosado et al. 2015). We are therefore justified in treating the GW source as monochromatic (Sesana et al. 2008; Sesana & Vecchio 2010; Ellis et al. 2012).

The amplitude tensor $H_{\mu\nu}$ has zero temporal components ($H_{0\mu} = H_{\mu 0} = 0$). The spatial part is

$$H_{ij} = h_+ e^+_{ij}(\boldsymbol{n}) + h_\times e^\times_{ij}(\boldsymbol{n}) , \tag{7}$$

where h_+ and $h_\times$ are the respective polarisation amplitudes. The plus and cross polarisation tensors e^+_{ij} and $e^\times_{ij}$ are uniquely defined by the principal axes of the wave, viz. the unit 3-vectors $\boldsymbol{k}$ and $\boldsymbol{l}$, according to

$$e^+_{ij}(\boldsymbol{n}) = k_i k_j - l_i l_j , \tag{8}$$

$$e^\times_{ij}(\boldsymbol{n}) = k_i l_j + l_i k_j . \tag{9}$$

The principal axes are in turn specified by the location of the GW source on the sky (via colatitude θ and azimuth ϕ) and the polarisation angle ψ according to

$$\begin{aligned}\boldsymbol{k} =&(\sin\phi\cos\psi - \sin\psi\cos\phi\cos\theta)\hat{\boldsymbol{x}}\\ &-(\cos\phi\cos\psi + \sin\psi\sin\phi\cos\theta)\hat{\boldsymbol{y}}\\ &+(\sin\psi\sin\theta)\hat{\boldsymbol{z}}\end{aligned} \tag{10}$$

$$\begin{aligned}\boldsymbol{l} =&(-\sin\phi\sin\psi - \cos\psi\cos\phi\cos\theta)\hat{\boldsymbol{x}}\\ &+(\cos\phi\sin\psi - \cos\psi\sin\phi\cos\theta)\hat{\boldsymbol{y}}\\ &+(\cos\psi\sin\theta)\hat{\boldsymbol{z}}\end{aligned} \tag{11}$$

where e.g. $\hat{\boldsymbol{x}}$ is a unit vector in the direction of the x-axis. The direction of GW propagation is related to the principal axes by

$$\boldsymbol{n} = \boldsymbol{k}\times\boldsymbol{l} . \tag{12}$$

2.2.2 *Measurement equation*

TK: Does this subsection needs a better name?
TK: this subsection has been overhauled per comments from AM. The structure is now:
1. Radio pulses described by general geometric object p
2. Shift in p due to a GW (no derivation, just definition of terms)
3.Relate shift in p to a shift in f by clarifying that $u = (1, 0, 0, 0)$ for PSR and observer.
4. Give final measurement equation

In general radio pulses from a pulsar are transmitted as amplitude modulations of a radio-frequency carrier wave. They are described by the geometric object $\vec{p}$ which we can identify as the 4-momentum of the radio photon. The presence of a GW induces a shift in the temporal component of the covariant 4-momentum between the emitter and the observer, i.e. $\Delta p_t = p_t|_\mathrm{observer} - p_t|_\mathrm{emitter}$, as (e.g. Maggiore 2018)

$$\Delta p_t = \frac{\omega}{2}\frac{h_{ij}(t;\boldsymbol{x}=0)q^i q^j}{(1+\boldsymbol{n}\cdot\boldsymbol{q})}\left(1 - e^{i\Omega(1+\boldsymbol{n}\cdot\boldsymbol{q})d}\right) \tag{13}$$

where ω is the angular pulse frequency ($= 2\pi f_\mathrm{p}$) measured in the momentarily comoving reference frame (MCRF) of an observer, $h_{ij} = g_{ij} - \eta_{ij}$, $\boldsymbol{q}$ is the unit vector connecting the observer and the pulsar and d is the distance to the pulsar. We take the pulsar location $\boldsymbol{q}$ to be constant i.e. $\boldsymbol{q}$ is not a function of time. In practice the pulsar locations vary with respect to the Earth but are constant with respect to the SSB. This barycentering correction is typically applied when generating TOAs using e.g. TEMPO2 and related timing

software. Generally the measured frequency of a photon recorded by an observer who is travelling with 4-velocity $\vec{u}$ is given by the coordinate-independent expression:

$$f = p_\alpha u^\alpha \ . \tag{14}$$

Due to the kinematical corrections from the barycentering process,

$$u^\alpha|_{\rm emitter} = u^\alpha|_{\rm receiver} = (1, 0, 0, 0) \tag{15}$$

where the perturbations to $\vec{u}$ from the GW are of higher order and neglected. In this case the shift in the momentum from Equation 13 can be related to a shift in the frequency as,

$$f_{\rm m}^{(n)}(t) = f_{\rm p}^{(n)}(t-d)g^{(n)}(t) \tag{16}$$

where TK: what is the best notation here to give q^i an (n) superscript?

$$g^{(n)}(t) = 1 - \frac{1}{2}\frac{h_{ij}(t;\boldsymbol{x}=0)q^i_{(n)}q^j_{(n)}}{(1+\boldsymbol{n}\cdot\boldsymbol{q}^{(n)})}\left(1 - e^{i\Omega\left(1+\boldsymbol{n}\cdot\boldsymbol{q}^{(n)}\right)d^{(n)}}\right) \tag{17}$$

It is will also prove instructive to express Eq. 17 in a trigonometric form as, or in a trigonometric form

$$g^{(n)}(t) = 1 - \frac{1}{2}\frac{H_{ij}q^i_{(n)}q^j_{(n)}}{(1+\boldsymbol{n}\cdot\boldsymbol{q}^{(n)})} \times \left[\cos(-\Omega t + \Phi_0) - \cos\left(-\Omega t + \Phi_0 + \Omega\left(1+\boldsymbol{n}\cdot\boldsymbol{q}^{(n)}\right)d\right)\right] \tag{18}$$

Equations 16, 18, 17 define a measurement equation that relates the intrinsic pulsar spin frequency to the radio pulse frequency measured by an observer on Earth.

3 SIGNAL TRACKING AND PARAMETER ESTIMATION

The set of static parameters $\bar{\theta}$ of the model in Section 2 cane be separated into parameters which correspond to the intrinsic frequency evolution of the pulsar and parameters of the GW source, i.e.

$$\bar{\theta} = \bar{\theta}_{\rm psr} \cup \bar{\theta}_{\rm gw} \tag{19}$$

with

$$\bar{\theta}_{\rm psr} = \left\{\gamma^{(n)}, f^{(n)}_{\rm em}(t_1), \dot{f}^{(n)}_{\rm em}(t_1), d^{(n)}, \sigma^{(n)}\right\}_{1\leqslant n\leqslant N} \tag{20}$$

and

$$\bar{\theta}_{\rm gw} = \{h_+, h_\times, \delta, \alpha, \psi, \Omega, \Phi_0\} \ . \tag{21}$$

We can reparameterize the two GW polarisation strains in terms of the GW amplitude h_0 and the system inclination ι

$$h_+ = h(1+\cos^2\iota) \tag{22}$$

$$h_\times = -2h\cos\iota \tag{23}$$

where ι is the angle between the normal to the SMBHB orbital plane, $\boldsymbol{L}$ and the observer line of sight, i.e. $\cos\iota = \boldsymbol{n}\cdot\boldsymbol{L}$. Henceforth we use the parametrisation in terms of h_0 and ι. For a PTA dataset containing N pulsars we have $7+5N$ parameters to estimate. Typically the pulsar parameters are better constrained than the GW parameters: for example estimates of pulsar distances are accurate to $\sim 10\%$, but we have no prior information on the source location (Cordes & Lazio 2002; Verbiest et al. 2012; Desvignes et al. 2016; Yao et al. 2017).The variance of the measurement noise Σ can be estimated approximately from the root-mean-square amplitude of phase residuals and we do not treat it as a parameter to be inferred in this work.

In this section we present a new method to infer $\bar{\theta}$ and calculate the marginal likelihood (i.e. the model evidence). In Section 3.1 we outline how noisy measurements of the pulsar frequency $f_{\rm m}^{(n)}(t)$ can be used to estimate the hidden state sequence $f_{\rm p}^{(n)}(t)$ using a Kalman filter. In Section 3.2 we demonstrate how to deploy the Kalman filter in conjunction with a nested sampler to perform Bayesian inference of the model parameters and calculate the model evidence. Model selection and the specification of the null model is described in Section 3.3.

3.1 Kalman filter

The Kalman filter (Kalman 1960) is an algorithm for recovering the most likely evolution of a set of system state variables, $\boldsymbol{X}$ given some noisy measurements $\boldsymbol{Y}$. It is a common technique in signal processing that has been applied successfully in neutron star astrophysics (e.g. Meyers et al. 2021b; Melatos et al. 2021). In this work we use the linear Kalman filter which assumes a linear relation between $\boldsymbol{X}$ and $\boldsymbol{Y}$. Whilst the measurement equation, Eq. 16, is non-linear in the static parameters it is linear in the state and measurement variables, $f_{\rm p}^{(n)}$ and $f_{\rm m}^{(n)}$ respectively. Extension to non-linear problems is straightforward using either an extended Kalman filter (Zarchan & Musoff 2000), the unscented Kalman filter (Wan & Van Der Merwe 2000) or the particle filter (Simon 2006).

The full set of Kalman recursions is presented in Appendix A. At each discrete timestep $i = 1, ..., M$, the Kalman filter returns an estimate of the state variables, $\hat{\boldsymbol{X}}_i$, and the covariance of those estimates $\boldsymbol{P}_i$. The filter tracks the error in its predictions of $\boldsymbol{X}_i$ by projecting the state predictions back into measurement space, $\hat{\boldsymbol{X}}_i \mapsto \hat{\boldsymbol{Y}}_i$, via the measurement equation. The measurement predictions can then be compared aganst the true observed noisy measurements to get a residual $\boldsymbol{\epsilon}_i = \boldsymbol{Y}_i - \hat{\boldsymbol{Y}}_i$, sometimes termed the "innovation". The Kalman filter also calculates the uncertainty in $\boldsymbol{\epsilon}_i$ via the innovation covariance $\boldsymbol{S}_i = \langle\boldsymbol{\epsilon}_i\boldsymbol{\epsilon}_i^{\rm T}\rangle$. The Gaussian log-likelihood can then be calculated at each timestep,

$$\log\mathcal{L}_i = -\frac{1}{2}\left(N\log 2\pi + \log|\boldsymbol{S}_i| + \boldsymbol{\epsilon}_i^{\rm T}\boldsymbol{S}_i^{-1}\boldsymbol{\epsilon}_i\right) \tag{24}$$

with the total log-likelihood the sum over all timesteps, i.e.

$$\log\mathcal{L} = \sum_{i=1}^{i=M}\log\mathcal{L}_i \tag{25}$$

The likelihood $\mathcal{L}$, along $\hat{\boldsymbol{X}}$ and $\hat{\boldsymbol{Y}}$, are functions of the static parameters of the model, $\bar{\theta}$. If the estimates of the system parameters, $\hat{\theta}$, that we pass to the Kalman filter are close to the true underlying parameters then the error in $\hat{\boldsymbol{X}}$, $\hat{\boldsymbol{Y}}$ is minimized and $\mathcal{L}$ is maximised. This is illustrated in Figure 1a; given a data timeseries of the measured pulsar frequency the Kalman filter is able to recover the hidden state evolution with high fidelity. Conversely, if $\hat{\theta}$ is not close to $\bar{\theta}$ then the filter is unable to recover the state evolution. This is demonstrated in Figure 1b where the failure of the filter to track the hidden state is evident.

3.2 Nested Sampling

We can use the likelihood returned by the Kalman filter, Eq 25, in conjunction with likelihood-based inference methods to estimate the

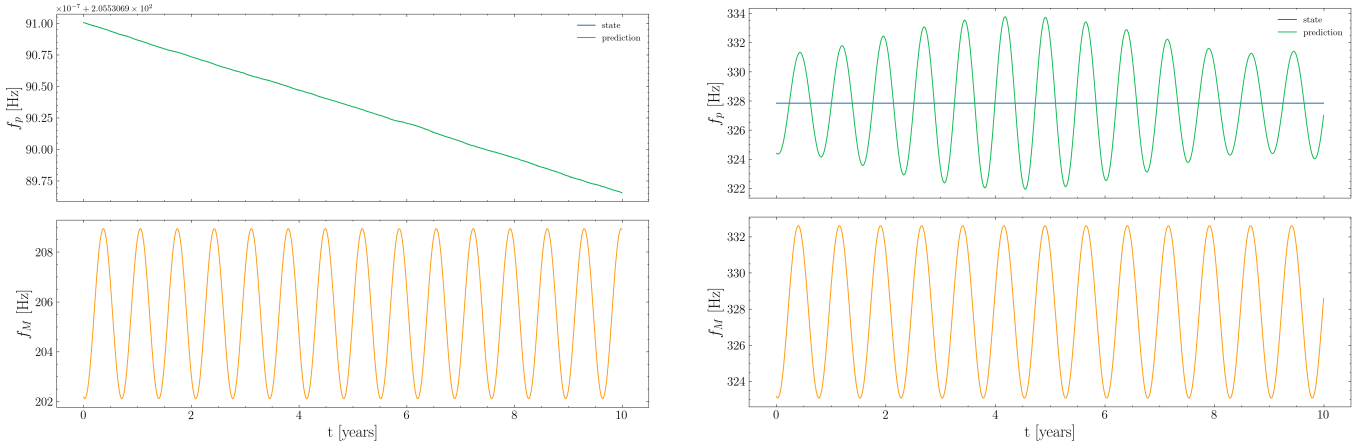

(a) Using correct parameters

(b) Using incorrect parameters

Figure 1. Application of a Kalman filter to recover the intrinsic frequency states (top panels) given a measured frequency signal (bottom panels) which has been modulated by the presence of a gravitational wave. In the case where the parameters of the filter are accurate (subfigure (a)) the underlying states are also recovered accurately. Conversely, when the parameters fed to the filter are inaccurate (subfigure (b)) the filter cannot recover the state. TK: this needs to be just one stacked figure.

posterior distribution of $\bar{\theta}$ by Bayes' Rule,

$$p(\bar{\theta}|\boldsymbol{Y}) = \frac{\mathcal{L} \cdot \pi(\theta)}{\mathcal{Z}} \tag{26}$$

where $\pi(\theta)$ is the prior distribution on $\bar{\theta}$ and $\mathcal{Z}$ is the marginalised likelihood, or evidence

$$\mathcal{Z} = \int \mathcal{L}\pi(\theta) d\theta \tag{27}$$

In order to estimate the posterior distribution and the model evidence we use nested sampling (NS, Skilling 2006). Nested sampling is an integration algorithm used for evaluating marginalised likelihood integrals, of the form given by Eq. 27, that also returns samples from the posterior $p(\bar{\theta}|\boldsymbol{Y})$. The primary advantage of nested sampling is the ability to compute this evidence integral, which is key for model selection, and proves difficult without considerable extra cost for the usual Markov Chain Monte Carlo (MCMC) approaches. Nested sampling is also typically less computationally intensive than MCMC and can handle multi-modal problems (Ashton et al. 2022). For these reasons, it has enjoyed widespread adoption in the physical sciences, particularly within the cosmological community (Mukherjee et al. 2006; Feroz & Hobson 2008; Handley et al. 2015), but has also commonly been applied in astrophysics (Buchner 2021), particle physics (Trassinelli 2019) and materials science (Pártay et al. 2009). Within this work we exclusively use nested sampling for Bayesian parameter estimation and model selection.

Multiple nested sampling libraries exist. For gravitational astrophysics it is common to use the dynesty sampler CITE, via the Bilby gravitational wave inference library and we continue to follow this precedent. TK: update text here from other version

3.3 Model selection

The evidence integral returned by nested sampling is the probability of the data $\boldsymbol{Y}$ given a particular model $\mathcal{M}$. This enables us to compare competing models via a Bayes factor,

$$\beta = \frac{\mathcal{Z}(\mathcal{M}_1)}{\mathcal{Z}(\mathcal{M}_0)} \tag{28}$$

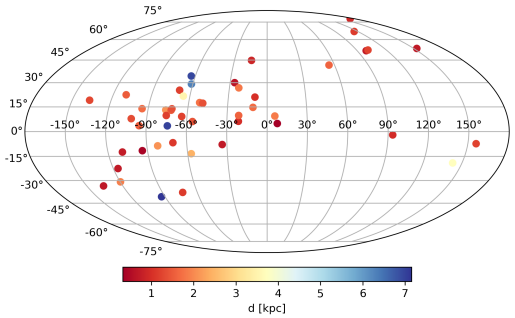

Figure 2. Spatial distribution and distances of NANOGrav pulsars

where the subscript index identifies a particular model. Throughout this work we take $\mathcal{M}_1$ to be the complete model defined in Section 2. $\mathcal{M}_0$ is our null model that assumes there is no GW in the data. This is equivalent to setting $g^{(n)}(t)$ from Equation 17, 18 = 1. The Bayes factors we quote in this paper therefore quantify whether the data shows evidence for a GW compared to no GW.

4 TESTS WITH SYNTHETIC DATA

We go on to discuss our choice of pulsars to make up our PTA in Section 4.2, before deploying these techniques in Sections 4.3 , 4.4 for parameter estimation and model selection.

4.1 Practical considerations

heterodyeing

pulsar terms For now we will consider the measurement noise to be known, although in principle this too could be estimated.

4.2 PTA pulsars

With our Kalman filter and nested sampling techniques in hand, in order to proceed it is necessary to specify a PTA configuration. As discussed, multiple separate PTA detectors exist under the umbrella

Parameter	Value
ω	5×10^{-7}
α	1.0
δ	1.0
ψ	2.50
ι	1.0
Φ_0	0.20
h	1e-2
$\sigma_{\rm p}$	10^{-13}
$\sigma_{\rm m}$	10^{-10}
T_{obs}	10 years
Δt	7 days

Table 1. GW parameters used for generating synthetic data. There is nothing special about these parameters - they are just chosen arbitrarily.

of the IPTA. Going forward we will take the 47 pulsars that make up the NANOGrav PTA (Arzoumanian et al. 2020b). NANOGrav is selected simply as a well-representative example of the typical pulsars that make up a PTA. Our results and formulation are not contingent on the choice of PTA, and naturally extend to other PTAs or PTAs with more pulsars.

Within our state-space formulation, the pulsar evolution is governed by a set of 5 parameters, $\bar{\theta}_{\rm PSR}$ for each pulsar. The parameters $f_{\rm EM}(0)$,$\dot{f}_{\rm EM}(0)$ and d are well specified via existing pulsar datasets. We take the frequency and frequency derivative as returned from the pulsar datasets to simply be the values now at $t = 0$. The pulsar distances are also known, though less well constrained. Going forward we take the distances retuned from the datasets as the true values of the pulsars that make up our synthetic PTA. The specification of γ and σ are more involved. γ specifies an effective timescale of reversion to the mean TK: Need some discussion and though on how to choose these two parameters to be astrophysically reasonable c.f. A. Vargas

4.3 Parameter estimation

We are now in a position to try to infer the parameters of a GW system. We take our NANOGrav PTA and create a synthetic noisy dataset using the parameters described in Table 1. Given this synthetic data, we can try to use our KF + NS approach to recover some of the parameters. The results for inference on 5 parameters, $\omega.\Phi_0, \psi, \iota, h$ are shown in Fig 3. TK: likelihood plots for each parameter could also be of interest to include here? Need to expand this section greatly for more astrophysical systems and more unknown parameters

4.4 Detection

In addition to estimating the parameters of the system, we are also interested in how detectable a GW is using PTA + state space method. We can use our state-space tools to try to solve the problem of GW detection with a PTA i.e. *"Is there evidence of a GW in my data?"*We can frame this as a model selection procedure where we have two models/hypotheses:

- Null Model, M_0. There is no GW in the data. In this case the measurement model of the Kalman filter simply returns the frequency states i.e. $g(t, \theta) = 0$
- Alternative model, M_1. There is a GW in the data. The measurement model uses the full expression for $g(t, \theta)$

In order to accept the alternative hypothesis M_1 over M_0 there are two approaches we could take:

(i) The first is a fully Bayesian search over all the parameters for each model, calculating the evidence for each model and then determining the Bayes ratio. This is perhaps the most consistent way, but it is obviously expensive and at this stage we are keen to explore how detectability varies with e.g. GW strain.

(ii) The second method is to recognize that M_0 and M_1 are hierarchically nested models and we can perform a likelihood ratio test. That is, given the maximum likelihood estimators $\hat{\theta}$ of the true parameters θ, the likelihood of each model can be calculate. These likelihoods are just point estimates of the Bayes factor numerator/denominators. They can then be compared via the likelihood ratio Λ.

Given the cheap cost we proceed with the second method. For the likelihood ratio test we do not perform any kind of maximum likelihood search over the parameters for each of the models. Instead we just artificially set the maximum likelihood estimators to be equal to the true parameters of the system i.e. $\hat{\theta} = \theta$. We assume that any maximum likelihood algorithm would converge to these parameters. This is obviously an oversimplification but will serve our purposes for now.

Interpreting the likelihood ratio Λ also needs some consideration, since we have to account for the increased model complexity of M_1. Bayes factors penalise complexity by construction since one must integrate over a larger parameter space. There are many different ways to do this - fot now we will consider two: Akaike information criterion (AIC) and Wilks Theorem. For the latter, Wilks' Theorem which states that for a large number of samples [1] the distribution of the test statistic approaches the chi-squared distribution under the null hypothesis i.e.

$$2 \log \Lambda \rightarrow \chi^2 \tag{29}$$

One can then compute p-values where the number of degrees of freedom is equal to the difference in the number of parameters of the two models; M_1 has 7 extra parameters over M_0 corresponding to the 7 parameters of $\bar{\theta}_{\rm GW}$. With 7 degrees of freedom and a target tolerance of 5(1) % the test statistic is $\sim 14(18.5)$.

An alternative approach is to use the AIC which is given by,

$$\text{AIC} = 2k - 2 \log \mathcal{L} \tag{30}$$

where k is the number of degrees of freedom. The AIC can be computed for each model and the model with the minimum AIC is preferred. This can be straightforwardly mapped into a relative condition

$$\log \mathcal{L}_1 - \log \mathcal{L}_0 > 7 \tag{31}$$

Note this is the same as the Wilks case!

5 DISCUSSION

Points to discuss:

- Non constant time sampling? Different pulsars sampled at different times...

[1] What counts as large? See https://www.osti.gov/servlets/purl/1529145

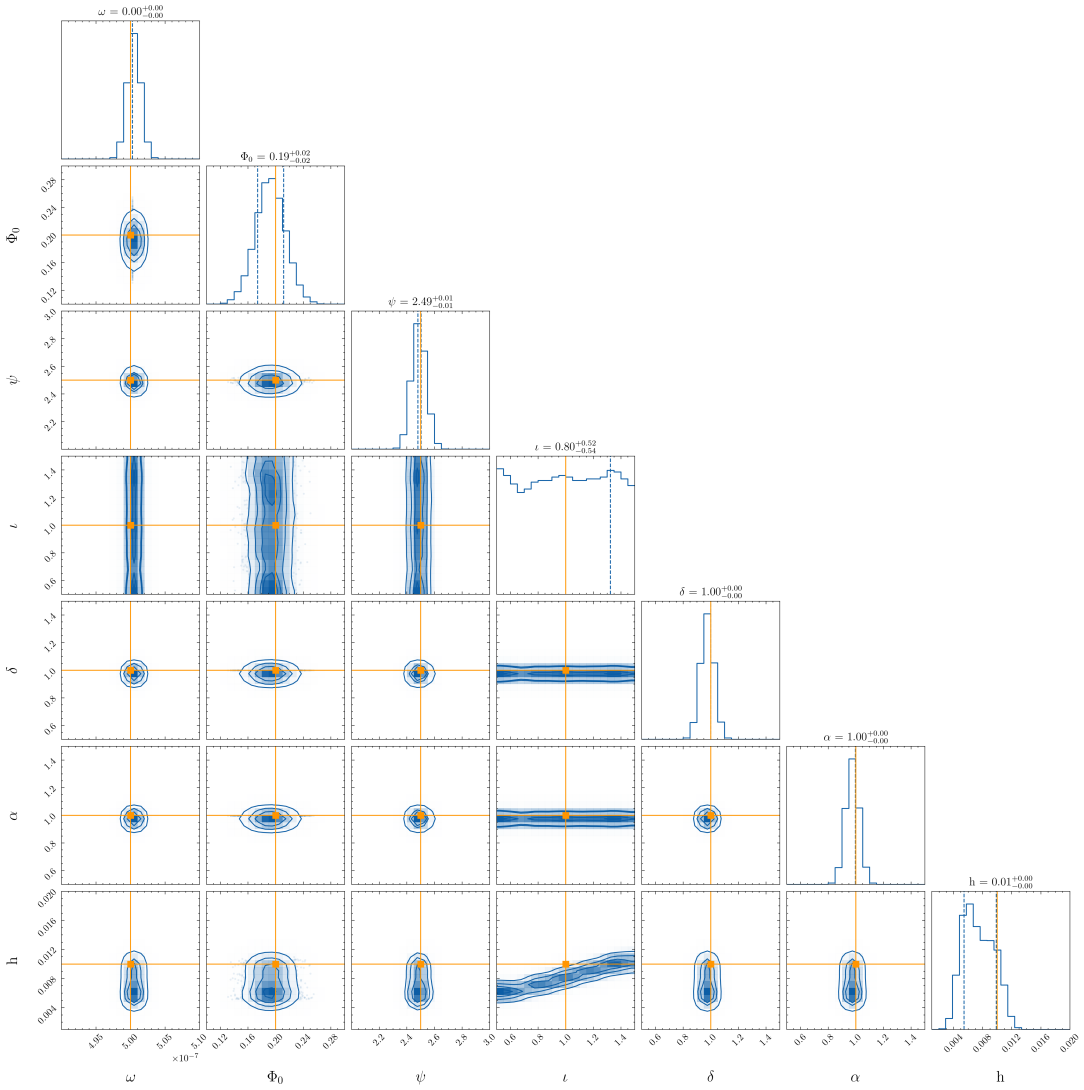

Figure 3. Example corner plot. Aside: for this run the σ_p value fed to the filter is different from that used to generate the data.

6 CONCLUSION

Questions

- PTAs like MSPs for small timing noise. Can we get away with large timing noise, and use more pulsars? Some pulsars are more useful than others, e.g. arXiv 2211.03201
- Can we also estimate radiometer noise? Is this useful?

APPENDIX A: KALMAN RECURSION EQUATIONS

The linear Kalman filter operates on temporally discrete measurements which are related to unobservable system states via a linear transformation

$$\bar{z} = \bar{H}\bar{x} + \bar{v} \tag{A1}$$

where $\bar{H}$ is the measurement matrix and $\bar{v}$ is a Gaussian measurement noise. The underlying states evolve according to are the state-space dynamical equation

$$\dot{\bar{x}} = \bar{F}\bar{x} + \bar{G}\bar{u} + \bar{w} \tag{A2}$$

for the system dynamics matrix,$\bar{F}$, control model G, control vector $\bar{u}$, and w a stochastic zero-mean process. By comparison with the preceding equations, Eqs. A9 - **??**, it is immediately obvious how our state space model maps onto the Kalman filter structure. Specifically, our states are just the N intrinsic pulsar frequencies $\bar{x} = (f_1, f_2, ...f_N)$ whilst our measurements are the N measured pulse frequencies $\bar{z} = (f_1^{(M)}, f_2^{(M)}, ...f_N^{(M)})$. If we specialize to the case of constant time sampling between our observations, Δt, then for our formulation the components that make up the Kalman filter are as follows:

$$F_i = F_{i+1} = e^{-\gamma \Delta t} \tag{A3}$$

$$T_i = \int_{t_i}^{t_{i+1}} e^{A(t_{i+1}-t')} N(t') dt' \tag{A4}$$

$$= f_{\rm EM}(0) + \dot{f}_{\rm EM}(0)(\Delta t + t_i) - e^{-\gamma \Delta t}\left(f_{\rm EM}(0) + \dot{f}_{\rm EM}(0) t_i\right) \tag{A5}$$

$$H_i = 1 - A(\theta_{\rm GW}) \cos(-\Omega t_i (1 + n \cdot q) + \Phi_0) \tag{A6}$$

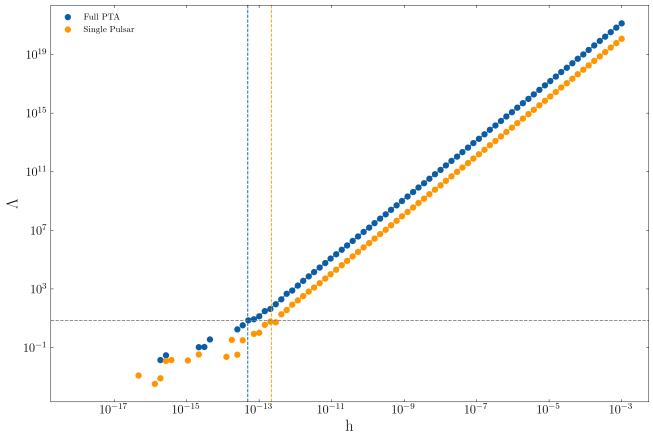

Figure 4. Likelihood ratio vs strain for *(a)* full PTA and *(b)* a single randomly chosen pulsar. Horizontal dashed line shows the minimum detectable cutoff, vertical dashed lines are the corresponding GW strains.

where the i subscript labels the value at the i-th timestep, and A is a constant that is given by Eq. **??**.

The Kalman filter includes the effect of process noise $\bar{w}$ and the measurement noise $\bar{v}$ via the definition of a process noise matrix $Q = E[ww^T]$ and a measurement noise matrix $R = E[vv^T]$, which have the discrete form,

$$Q_i\delta_{ij} = \langle \eta_i \eta_j^T \rangle = \frac{-\sigma^2}{2\gamma}\left(e^{-2\gamma\Delta t} - 1\right) \tag{A7}$$

$$R_i = R_{i+1} = \Sigma^2 \tag{A8}$$

The above equations, Eqs. A3 - A8, apply to an operation on a single state. The extension to N states is straightforward, since one just needs to construct a diagonal matrix for each of the Kalman components where each non-zero element corresponds to a separate pulsar frequency.

In Section **??** we present a discretised version of the model of Section 2 which maps onto the discretely sampled observable $f(\tau)|_{\rm Earth}$.

In order to make contact with discretely sampled data it is importnat to temporally discretise the model of Section 2

We can express the intrinsic frequency evolution, Eq. **??**, in a alternative form as, TK all this needs updating

$$df = \gamma f dt + N(t)dt + \sigma dB(t) \tag{A9}$$

where $\mathcal{A} = -\gamma$, $N(t) = \gamma(f_{\rm EM}(0) + \dot{f}_{\rm EM}(0)t) + \dot{f}_{\rm EM}(0)$ and $dB(t)$ denotes increments of Brownian motion (Wiener process). This equation is easily identified as an Ornstein-Uhlenbeck process which has a general solution given by (Gardiner 2009),

$$f(t) = e^{\mathcal{A}t}f(0) + \int_0^t e^{\mathcal{A}(t-t')}N(t')dt' + \int_0^t e^{\mathcal{A}(t-t')}\sigma dB(t') \tag{A10}$$

If we move from a solution in continuous time, t, to discrete time, TK: AM reccomends deligint tabe sy,bol $\bar{t} = (t_1, t_2, ..., t_K)$, then

$$f(t_{i+1}) = Ff(t_i) + T_i + \eta_i \tag{A11}$$

where

$$F_i = e^{\mathcal{A}(t_{i+1}-t_i)} \tag{A12}$$

$$T_i = \int_{t_i}^{t_{i+1}} e^{\mathcal{A}(t_{i+1}-t')}N(t')\,dt' \tag{A13}$$

$$\eta_i = \int_{t_i}^{t_{i+1}} e^{\mathcal{A}(t_{i+1}-t')}\sigma\,dt' \tag{A14}$$

if we specialise to the case of constatn time sampling

The discrete solution $f(\bar{t})$ to the intrinsic frequency can be related to the discrete measured frequency via Eq. **??** as,

$$f_M(\bar{t}) = f(\bar{t})g(\bar{\theta}, \bar{t}) + N_M \tag{A15}$$

where $g(\theta, t)$ can be expressed in a trigonometric form as

$$X = 1 - \frac{1}{2}\frac{H_{ij}q^i q^j}{(1+\bar{n}\cdot\bar{q})}\left[\cos(-\Omega\tau + \Phi_0) - \cos(-\Omega\tau + \Phi_0 + \Omega(1+\bar{n}\cdot\bar{q})d)\right] \tag{A16}$$

whilst N_M is a Gaussian measurement noise that satisfies

$$\langle N_M(t)N_M(t')\rangle = \Sigma^2\delta(t-t') \tag{A17}$$

for variance Σ^2.

A1 References

REFERENCES

Agazie G., et al., 2023, ApJ, 951, L9
Allen B., 1997, in Marck J.-A., Lasota J.-P., eds, Relativistic Gravitation and Gravitational Radiation. pp 373–417 (arXiv:gr-qc/9604033), doi:10.48550/arXiv.gr-qc/9604033
Antonelli M., Basu A., Haskell B., 2023, MNRAS, 520, 2813
Antoniadis J., et al., 2022, MNRAS, 510, 4873
Antoniadis J., et al., 2023, arXiv e-prints, p. arXiv:2306.16224
Arzoumanian Z., et al., 2018, ApJ, 859, 47
Arzoumanian Z., et al., 2020a, ApJ, 900, 102
Arzoumanian Z., et al., 2020b, ApJ, 905, L34
Arzoumanian Z., et al., 2023, arXiv e-prints, p. arXiv:2301.03608
Ashton G., et al., 2022, Nature Reviews Methods Primers, 2, 39
Babak S., Sesana A., 2012, Phys. Rev. D, 85, 044034
Babak S., et al., 2016, MNRAS, 455, 1665
Bailes M., et al., 2020, Publications of the Astronomical Society of Australia, 37, e028
Baym G., Pethick C., Pines D., Ruderman M., 1969, Nature, 224, 872
Brook P. R., Karastergiou A., Buchner S., Roberts S. J., Keith M. J., Johnston S., Shannon R. M., 2013, The Astrophysical Journal Letters, 780, L31
Buchner J., 2021, The Journal of Open Source Software, 6, 3001
Burke-Spolaor S., et al., 2019, A&ARv, 27, 5
Caballero R. N., et al., 2016, MNRAS, 457, 4421
Christensen N., 2019, Reports on Progress in Physics, 82, 016903
Cordes J. M., Greenstein G., 1981, ApJ, 245, 1060
Cordes J. M., Lazio T. J. W., 2002, arXiv e-prints, pp astro–ph/0207156
Cordes J. M., Shannon R. M., 2010, arXiv e-prints, p. arXiv:1010.3785
D'Alessandro F., McCulloch P. M., Hamilton P. A., Deshpande A. A., 1995, MNRAS, 277, 1033
Desvignes G., et al., 2016, Monthly Notices of the Royal Astronomical Society, 458, 3341
Dunn L., et al., 2022, MNRAS, 512, 1469
Dunn L., Melatos A., Espinoza C. M., Antonopoulou D., Dodson R., 2023, MNRAS, 522, 5469
Ellis J. A., 2013, Classical and Quantum Gravity, 30, 224004
Ellis J. A., Cornish N. J., 2016, Phys. Rev. D, 93, 084048
Ellis J. A., Siemens X., Creighton J. D. E., 2012, ApJ, 756, 175
Espinoza C. M., Antonopoulou D., Dodson R., Stepanova M., Scherer A., 2021, A&A, 647, A25
Feroz F., Hobson M. P., 2008, MNRAS, 384, 449

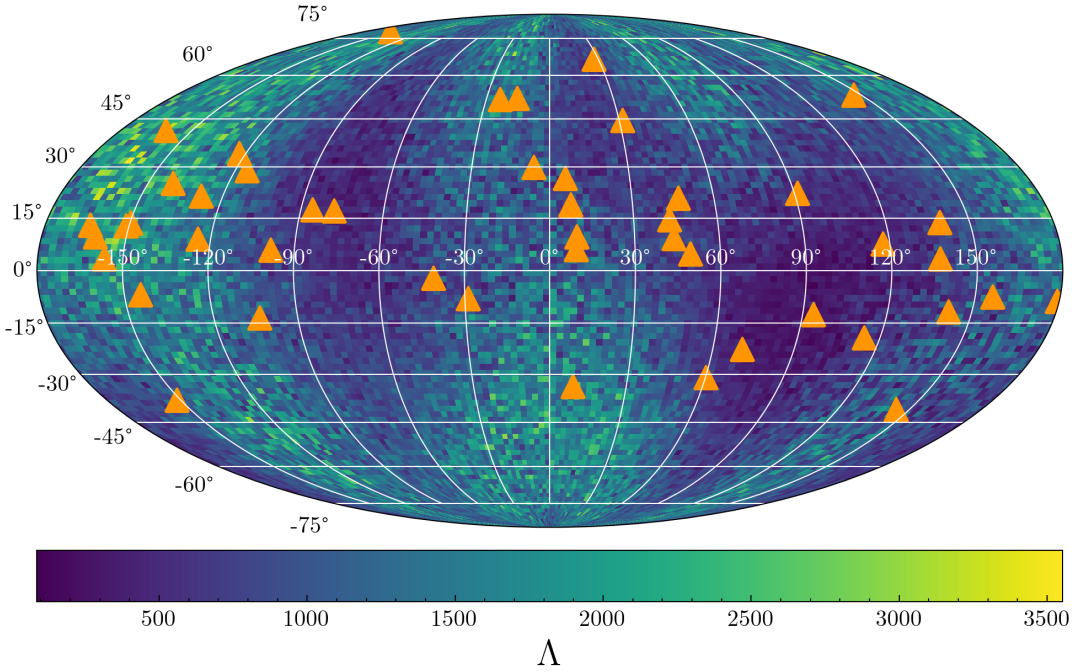

Figure 5. TK: Just a placeholder. Likelihood ratio for a given h. Maybe more interesting, but more expensive, to get minimum detectable h?

Gardiner C., 2009, Stochastic Methods: A Handbook for the Natural and Social Sciences. Springer Series in Synergetics, Springer Berlin Heidelberg, https://books.google.com.au/books?id=otg3PQAACAAJ

Goncharov B., et al., 2021, MNRAS, 502, 478

Greenstein G., 1970, Nature, 227, 791

Gügercinoğlu E., Alpar M. A., 2017, MNRAS, 471, 4827

Handley W. J., Hobson M. P., Lasenby A. N., 2015, MNRAS, 450, L61

Hellings R. W., Downs G. S., 1983, ApJ, 265, L39

Hobbs G., Lyne A. G., Kramer M., 2010, MNRAS, 402, 1027

Hobbs G., Dai S., Manchester R. N., Shannon R. M., Kerr M., Lee K.-J., Xu R.-X., 2019, Research in Astronomy and Astrophysics, 19, 020

Jaffe A. H., Backer D. C., 2003, The Astrophysical Journal, 583, 616

Jenet F. A., Lommen A., Larson S. L., Wen L., 2004, ApJ, 606, 799

Johnston S., Galloway D., 1999, Monthly Notices of the Royal Astronomical Society, 306, L50

Jones P. B., 1990, MNRAS, 246, 364

Kalman R. E., 1960, Journal of Basic Engineering, 82, 35

Kerr M., Hobbs G., Johnston S., Shannon R. M., 2015, Monthly Notices of the Royal Astronomical Society, 455, 1845

Kramer M., Lyne A. G., O'Brien J. T., Jordan C. A., Lorimer D. R., 2006, Science, 312, 549

Lam M. T., et al., 2019, ApJ, 872, 193

Lasky P. D., Melatos A., Ravi V., Hobbs G., 2015, MNRAS, 449, 3293

Lee K. J., Wex N., Kramer M., Stappers B. W., Bassa C. G., Janssen G. H., Karuppusamy R., Smits R., 2011, MNRAS, 414, 3251

Lentati L., et al., 2015, MNRAS, 453, 2576

Lower M. E., et al., 2021, MNRAS, 508, 3251

Lyne A., Hobbs G., Kramer M., Stairs I., Stappers B., 2010, Science, 329, 408

Maggiore M., 2018, Gravitational Waves: Volume 2: Astrophysics and Cosmology. Oxford University Press, doi:10.1093/oso/9780198570899.001.0001, https://doi.org/10.1093/oso/9780198570899.001.0001

McWilliams S. T., Ostriker J. P., Pretorius F., 2014, The Astrophysical Journal, 789, 156

Melatos A., Link B., 2014, MNRAS, 437, 21

Melatos A., Peralta C., Wyithe J. S. B., 2008, ApJ, 672, 1103

Melatos A., Dunn L. M., Suvorova S., Moran W., Evans R. J., 2020, ApJ, 896, 78

Melatos A., O'Neill N. J., Meyers P. M., O'Leary J., 2021, MNRAS, 506, 3349

Meyers P. M., Melatos A., O'Neill N. J., 2021a, MNRAS, 502, 3113

Meyers P. M., O'Neill N. J., Melatos A., Evans R. J., 2021b, MNRAS, 506, 3349

Mukherjee P., Parkinson D., Liddle A. R., 2006, ApJ, 638, L51

Pártay L. B., Bartók A. P., Csányi G., 2009, arXiv e-prints, p. arXiv:0906.3544

Parthasarathy A., et al., 2021, MNRAS, 502, 407

Peralta C., Melatos A., Giacobello M., Ooi A., 2006, ApJ, 651, 1079

Perera B. B. P., et al., 2019, MNRAS, 490, 4666

Rajagopal M., Romani R. W., 1995, ApJ, 446, 543

Ravi V., Wyithe J. S. B., Hobbs G., Shannon R. M., Manchester R. N., Yardley D. R. B., Keith M. J., 2012, ApJ, 761, 84

Ravi V., Wyithe J. S. B., Shannon R. M., Hobbs G., 2015, MNRAS, 447, 2772

Renzini A. I., Goncharov B., Jenkins A. C., Meyers P. M., 2022, Galaxies, 10, 34

Rosado P. A., Sesana A., Gair J., 2015, Monthly Notices of the Royal Astronomical Society, 451, 2417

Sanidas S. A., Battye R. A., Stappers B. W., 2012, Phys. Rev. D, 85, 122003

Sesana A., 2013, Classical and Quantum Gravity, 30, 224014

Sesana A., Vecchio A., 2010, Phys. Rev. D, 81, 104008

Sesana A., Vecchio A., Colacino C. N., 2008, Monthly Notices of the Royal Astronomical Society, 390, 192

Shannon R. M., Cordes J. M., 2010, ApJ, 725, 1607

Shannon R. M., et al., 2013, The Astrophysical Journal, 766, 5

Simon D., 2006, Optimal State Estimation: Kalman, H Infinity, and Nonlinear Approaches. Wiley-Interscience, USA

Skilling J., 2006, Bayesian Analysis, 1, 833

Sornette D., 2004, Critical phenomena in natural sciences : chaos, fractals selforganization and disorder : concepts and tools

Spiewak R., et al., 2022, Publ. Astron. Soc. Australia, 39, e027

Stairs I. H., Lyne A. G., Shemar S. L., 2000, Nature, 406, 484

Stairs I. H., et al., 2019, MNRAS, 485, 3230

Sykes B., Middleton H., Melatos A., Di Matteo T., DeGraf C., Bhowmick A., 2022, MNRAS, 511, 5241

Tarafdar P., et al., 2022, Publications of the Astronomical Society of Australia,

39, e053
Tiburzi C., 2018, Publ. Astron. Soc. Australia, 35, e013
Trassinelli M., 2019, Proceedings, 33
Urama J. O., Link B., Weisberg J. M., 2006, MNRAS, 370, L76
Vargas A., Melatos A., 2023, TBD, 1, 1
Verbiest J. P. W., Weisberg J. M., Chael A. A., Lee K. J., Lorimer D. R., 2012, ApJ, 755, 39
Verbiest J. P. W., Osłowski S., Burke-Spolaor S., 2021, in , Handbook of Gravitational Wave Astronomy. p. 4, doi:10.1007/978-981-15-4702-7_4-1
Wan E., Van Der Merwe R., 2000, in Proceedings of the IEEE 2000 Adaptive Systems for Signal Processing, Communications, and Control Symposium (Cat. No.00EX373). pp 153–158, doi:10.1109/ASSPCC.2000.882463
Wyithe J. S. B., Loeb A., 2003, ApJ, 590, 691
Xue X., et al., 2021, Phys. Rev. Lett., 127, 251303
Yao J. M., Manchester R. N., Wang N., 2017, ApJ, 835, 29
Yardley D. R. B., et al., 2010, MNRAS, 407, 669
Zarchan P., Musoff H., 2000, Fundamentals of Kalman Filtering: A Practical Approach. Progress in astronautics and aeronautics, American Institute of Aeronautics and Astronautics, https://books.google.com.au/books?id=AQxRAAAAMAAJ
Zhu X. J., et al., 2014, MNRAS, 444, 3709
Zhu X.-J., et al., 2015, Monthly Notices of the Royal Astronomical Society, 449, 1650
Zhu X.-J., Wen L., Xiong J., Xu Y., Wang Y., Mohanty S. D., Hobbs G., Manchester R. N., 2016, Monthly Notices of the Royal Astronomical Society, 461, 1317
Zic A., et al., 2023, arXiv e-prints, p. arXiv:2306.16230
van Eysden C. A., Melatos A., 2010, MNRAS, 409, 1253

This paper has been typeset from a TEX/LATEX file prepared by the author.